11th ANKARA INTERNATIONAL AEROSPACE CONFERENCE **AIAC-2021-106**
8-10 September 2021 - METU, Ankara TURKEY

Prediction of the Nearfield Pressure Signature Using HEMLAB Algorithm

Hulya Sukas* and Mehmet Sahin†
Istanbul Technical University
Istanbul, Turkey

ABSTRACT

In this study, the NASA Concept 25D with Flow-Through Nacelle (C25F) proposed in the AIAA Sonic Boom Workshop has been studied in two different aspects. First part of this paper is about validating the vertex based finite volume algorithm named HEMLAB for the selected geometry in terms of aerodynamic forces and pressure signatures. The HEMLAB algorithm uses the quad-edge and half-edge data structures to enhance cache efficiency. The stability of the algorithm is improved using the PETSc library for fully implicit solutions. All algebraic equations including the turbulence equations are solved in a monolithic manner using the restricted additive Schwarz preconditioner combined with the FGMRES(m) Krylov subspace algorithm. The same simulations have also been performed with the Stanford open-source SU2 algorithm and it is proved that the results obtained using the HEMLAB and SU2 are in a good manner with each other. In addition, the effect of the grid quality and resolution issues on the aerodynamic loads has been shared on the AIAA Drag Prediction Workshop series (DPW). Therefore, within the scope of this study, it is decided to improve the mesh resolution to obtain better numerical results. However, increasing the mesh resolution will cause additional computing resources and long simulation times, so an anisotropic mesh adaptation process is carried out to improve the mesh resolution effectively. For this purpose, the INRIA pyAMG library is integrated with the SU2 solver and the obtained results are compared with the benchmark solutions. The validation of the numerical results is performed using the nearfield pressure signatures for NASA-C25F model.

INTRODUCTION

Reynolds-Averaged Navier–Stokes (RANS) based Computational Fluid Dynamic (CFD) methods have been used as a significant tool for many years in order to obtain numerical results for cruise conditions. However, CFD is still challenging for special flight conditions such as sonic boom cases. For this purpose, AIAA Sonic Boom Workshops [Park et al (2019)] are organized to understand capabilities of the current CFD solvers. In order to measure capabilities of our code, a validation study is performed on the first part of this paper. The HEMLAB algorithm [Akkurt and Sahin, (2017)] based on highly efficient edge-based data structure is applied to the NASA-C25F model that

*Grad. student, Istanbul Technical University, Faculty of Aeronautics and Astronautics, Email: sukas17@itu.edu.tr
†Prof., Istanbul Technical University, Faculty of Aeronautics and Astronautics, Email: msahin@itu.edu.tr

is proposed on the 2nd AIAA Sonic Boom Workshop (SBW2). Besides, the simulation under the same conditions is carried out using the Stanford open-source SU2 solver [Becker and Granzoto, (2018)] with the same initial mesh. The results obtained are compared with the reference data provided on the SBW2. The accurate simulation of the NASA-C25F model is still challenging due to relatively complex flow physics requiring relatively large number of mesh resolution. As an alternative solution, mesh adaption process can be considered to decrease the cost of flow simulations by systematically reducing discretization errors. Therefore, the anisotropic pyAMG library [Loseille, (2014)] is integrated with the SU2 solver and mesh adaptation method is used to validate the results of C25F model. In this approach, the Riemannian metric space defined by the metric field used while computing the edge lengths and element volumes inside the mesh generator. This metric field is determined with a Hessian of the variable that can be selected as Mach, pressure, entropy, etc. This multi-scale refinement approach is different from drag, lift, etc. based goal oriented refinement algorithms even though they lead to a more efficient algorithm having relatively fewer number of mesh resolutions. However, these approaches require the solution of adjoint problems as well. The present anisotropic approach is very similar to the work of [Park et al. (2019)] for Flow-through nacelle (C25F) and Powered nacelle (C25P) configurations. The present method is also applied to the JAXA High Lift configuration in [Sukas and Sahin, (2021)].

NUMERICAL APPROACH

The HEMLAB code is a vertex-based unstructured finite volume solver. In the current version of the code, the Roe scheme is used for the calculation of the inviscid fluxes while it uses the Green Gauss theorem for the derivation of primitive variables to compute the viscous flux at the midpoints of edges. The unweighted least squares interpolation is used to interpolate the conservative variables for inviscid fluxes. The classical one-equation Spalart-Allmaras [Spalart and Allmaras, (1994)] turbulence model without transition terms is implemented for the turbulence model and it is solved with the Navier-Stokes equations in a fully coupled manner. The Newton method with the first-order Euler explicit in time is used for the time integration. The numerical method is based on the quad-edge and half-edge data structures to enhance cache efficiency. The computational domain is subdived into sub-domains using the METIS library. The PETSc library is used for the solution of resulting algebraic equations using the restricted additive Schwarz preconditioner combined with the FGMRES(m) Krylov subspace algorithm. An ILU(0) preconditioner used within each sub-blocks. Currently, only tetrahedra, wedge, pyramids and hexahedra type elements can be used in three dimensions. The numerical methods differs from the SU2 solver where the weighted least squares is used for inviscid fluxes and the viscous fluxes are evaluated as the simple averages of the nodal values resulting from the least squares approach. In the present work, the Green-Gauss approach within the SU2 solver is employed for gradient evaluations due to its better stability on anisotropic tetrahedral elements. Regarding the mesh adaptation process, the anisotropic mesh refinement library pyAMG is integrated with the SU2 solver which is very similar to the HEMLAB algorithm. However, the current version of this code uses local Mach number as a sensor function and this causes some coarsening issues on the boundary layer around the separation regions where the velocity gradients are weak. Therefore, it has been modified using Mach number and minimum distance function as follows:

$$Mach\ Sensor = \beta Mach + \sum_{i=1}^{4} 0.25 e^{-100*10^{i}d}$$

With this improvement, mesh adaptation can start even without a boundary layer. In this study, four level-only distance level refinements were performed with an initial mesh that has no boundary layer. In this part, β value is taken as 0 . Then eight-level of refinement was done with including Mach number. Therefore, β is set as 1. Figure 1 shows the refinement process flow chart that is followed in this study.

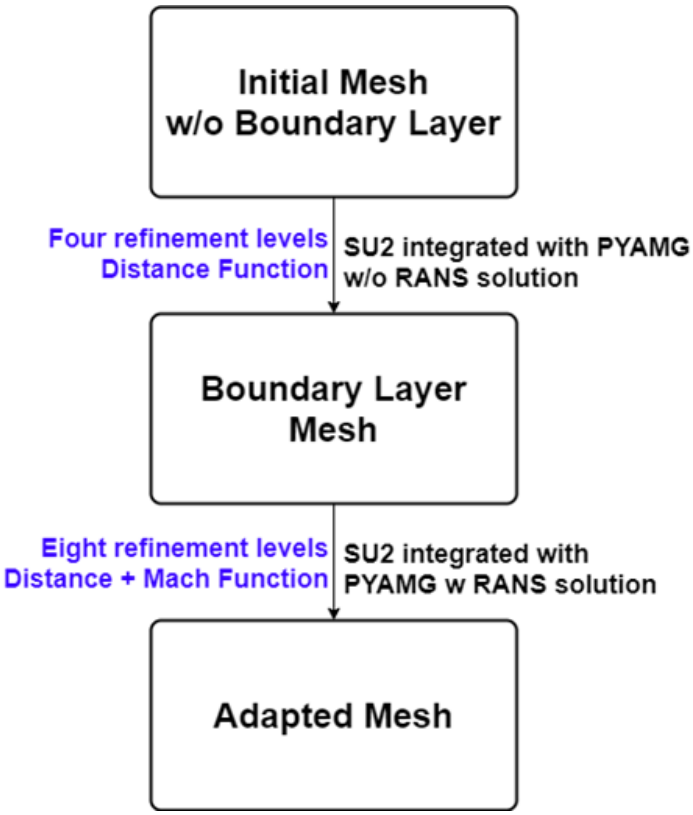

Figure 1: Flow chart for mesh adaptation process

RESULTS AND DISCUSSION

Initial Mesh Results

The initial numerical calculations are carried out on the grid provided by the SPW2 for the both SU2 and HEMLAB solvers. The computational mesh consists of 8927997 vertices and 24185029 unstructured elements. The free stream conditions are set to $M_\infty = 1.6$, $Re = 5.7x10^6$ and $\alpha = 0$. The computational domain is shown in Figure 2-[a], which is limited to the region behind the leading oblique shock. The computed nearfield pressure signatures are provided in Figure 2-[b] at one body length below the NASA-C25F model. It can be seen that the results are in a good agreement for the given range. The convergence of the aerodynamic loads are given on the Figure 3 and the converged values of the lift and drag coefficients can be found in Table 1. The values are very close the reference values in the literature. The computed skin friction lines with the pressure contours are also illustrated in Figure 4 for the mesh obtained from the SPW2 site.

Table 1: CL, CD and results

Results	SU2	HEMLAB	Ref.
C_L	0.06525	0.06565	0.06521
C_D	0.01465	0.01445	0.01463

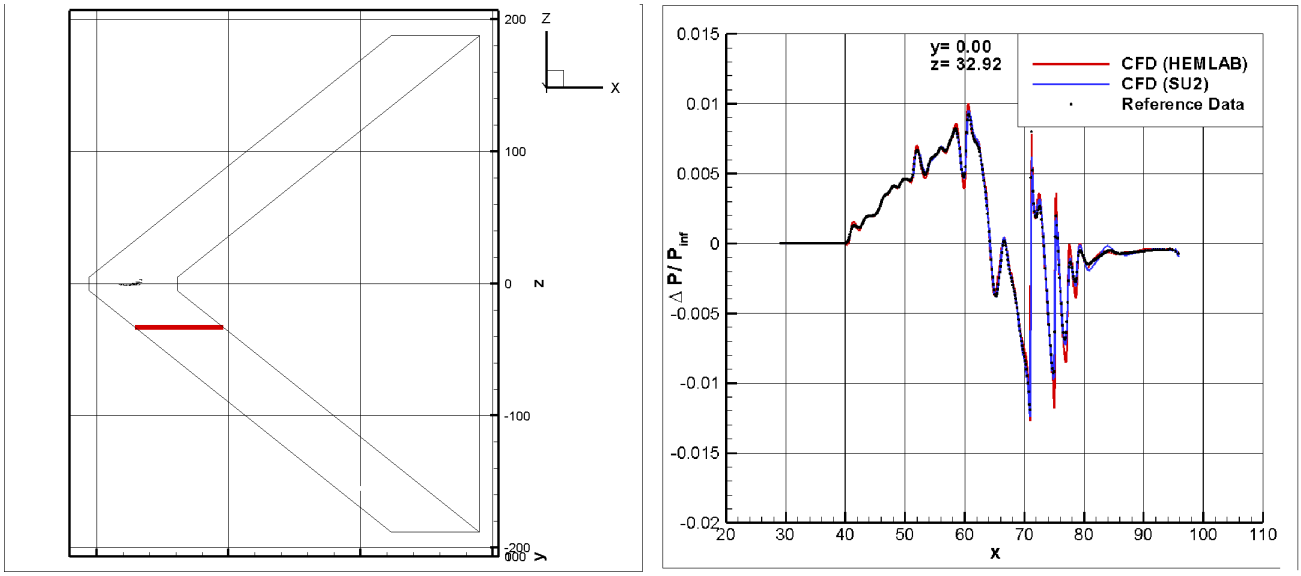

Figure 2: Nearfield pressure signature on the $z = -32.92$ and $y = 0$

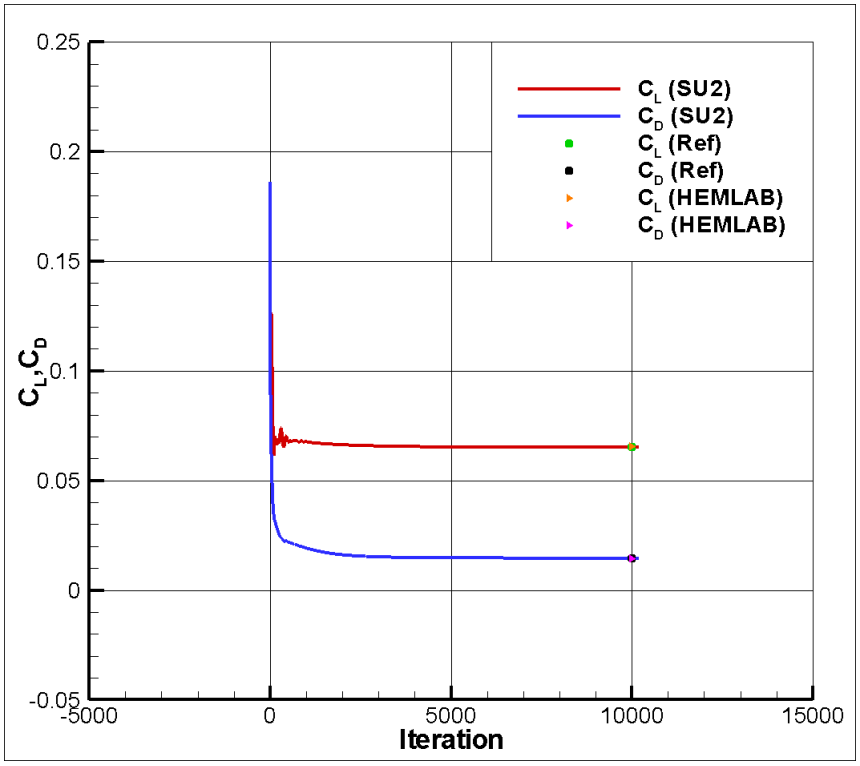

Figure 3: Convergence of the simulations in terms of C_L and C_D.

Adapted Mesh Results

As it is mentioned earlier, mesh adaptation study is also performed for the NASA C25F geometry to improve the numerical accuracy. For this purpose, four refinement level is done with only distance function while eight refinement level is performed with distance and Mach number together. The initial mesh has no boundary layer. In Figure 5, the pressure signatures around the nearfield are compared with the reference data [Park et. al.,2019] at the final mesh refinement process. The

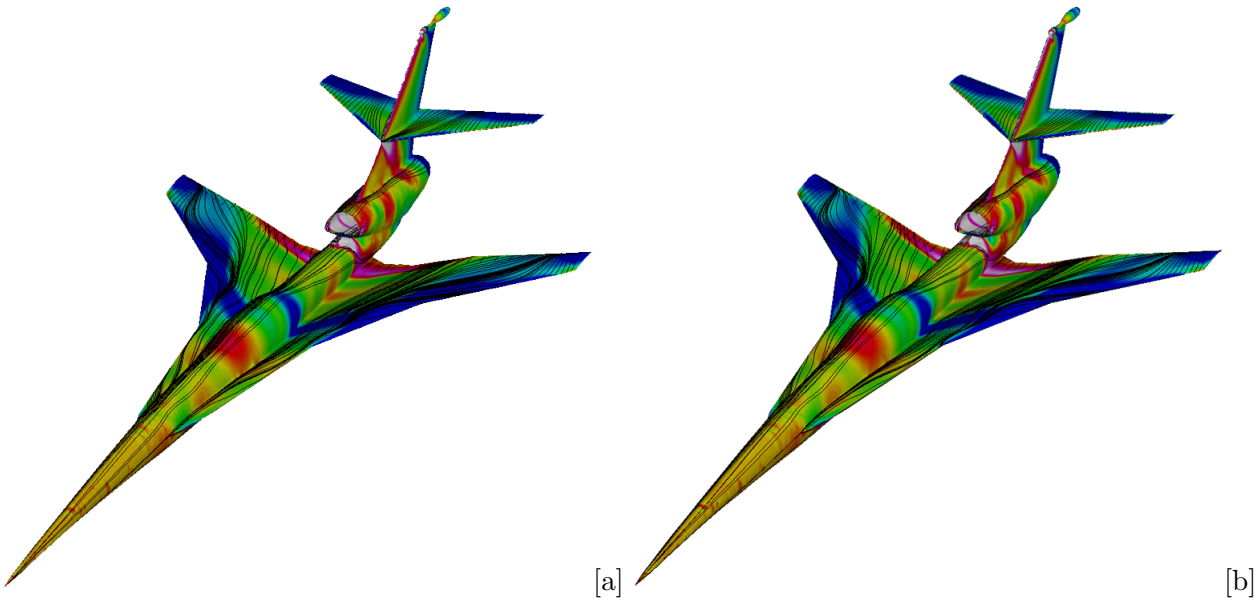

[a] [b]

Figure 4: Streamtraces on the main body for inital mesh with SU2 [a] and HEMLAB [b].

result also shows relatively good agreement with relatively sharper pressure peaks. Mesh structure details can be found at the Table 2 for each refinement level. Figures given below clearly shows the sonic boom distribution behind the supersonic aircraft at given planes. The three-dimensional shock waves and wakes can be clearly seen from Figure 6 at $x = 40$ plane. The wake structure is more observable in Figure 7 at $x = 50$ plane. The oblique shocks can be seen in Figure 8 with boundary layers and wakes at the $y = 0$ (symmetry) plane. It should be noted that, the contours for these figures shows the Mach number distribution on the flow domain. The shock waves, boundary layer and wakes are relatively well captured. In order to show the skin friction lines around the main body Figure 9 can be examined for the adapted mesh. The adapted pressure counter shows the shock locations more clearly.

Table 2: Refinement Data for AoA=0.0.

Refinement Level (Sensor Function)	Number of Vertices	Number of Elements	Number of Surface Elements
ite0 (Initial Mesh)	1,234,361	6,952,847	409,124
ite1 (Distance)	7,091,669	41,770,425	492,226
ite2 (Distance)	6,508,946	38,075,421	616,420
ite3 (Distance)	6,405,078	37,210,065	768,742
ite4 (Distance)	6,821,093	39,431,638	928,002
ite5 (Distance + Mach)	9,367,084	54,553,538	990,048
ite6 (Distance + Mach)	11,929,423	69,701,009	1,080,150
ite7 (Distance + Mach)	13,607,090	79,709,209	1,089,906
ite8 (Distance + Mach)	15,331,979	90,030,603	1,061,362
ite9 (Distance + Mach)	26,080,137	153,939,645	1,178,558
ite10 (Distance + Mach)	33,067,075	195,354,057	1,328,346
ite11 (Distance + Mach)	39,056,909	230,915,671	1,467,270
ite12 (Distance + Mach)	44,363,479	262,426,179	1,575,332

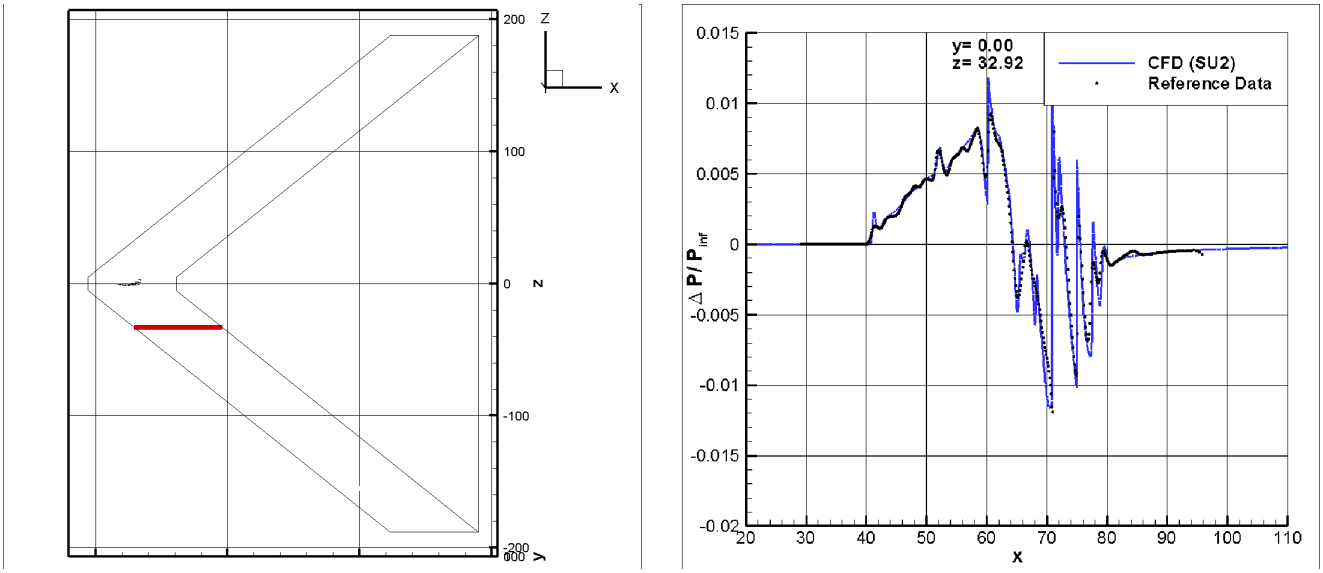

Figure 5: Nearfield pressure signature on the $z = -32.92$ and $y = 0$

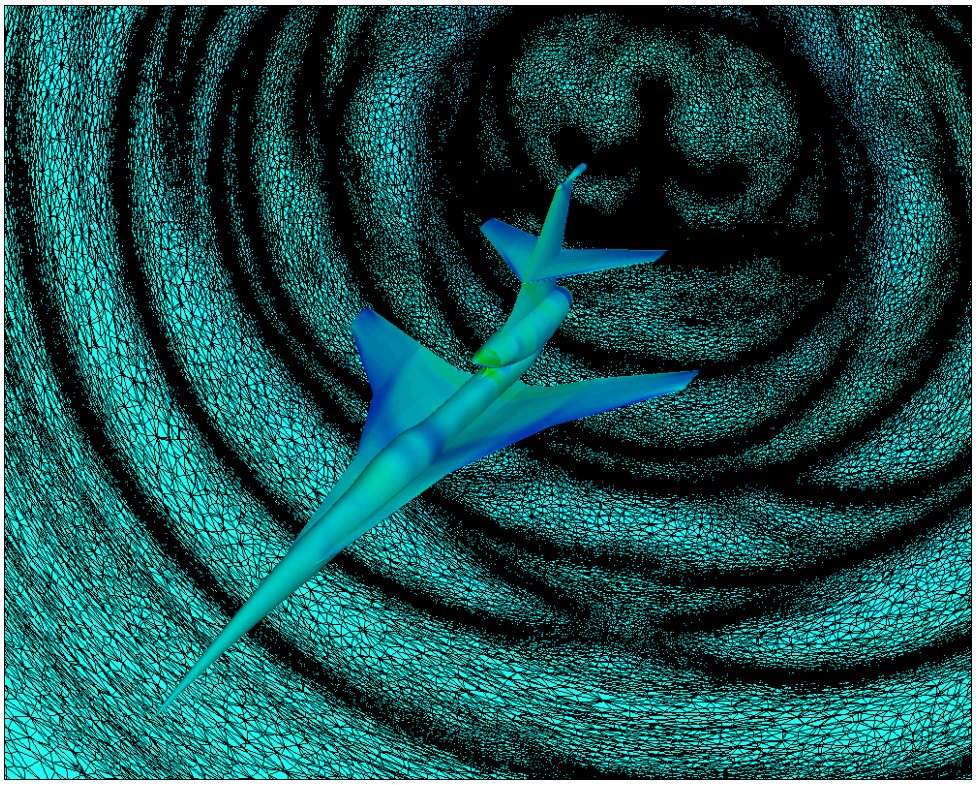

Figure 6: Wake region and sonic boom visualization at x=40

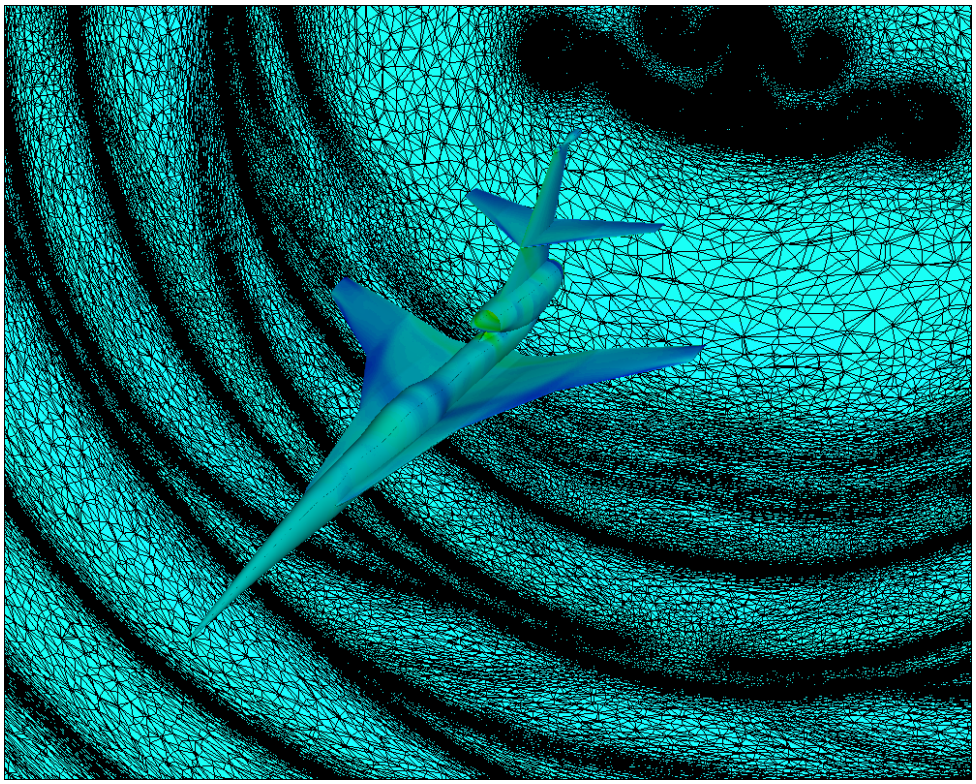

Figure 7: Wake region and sonic boom visualization at x=50

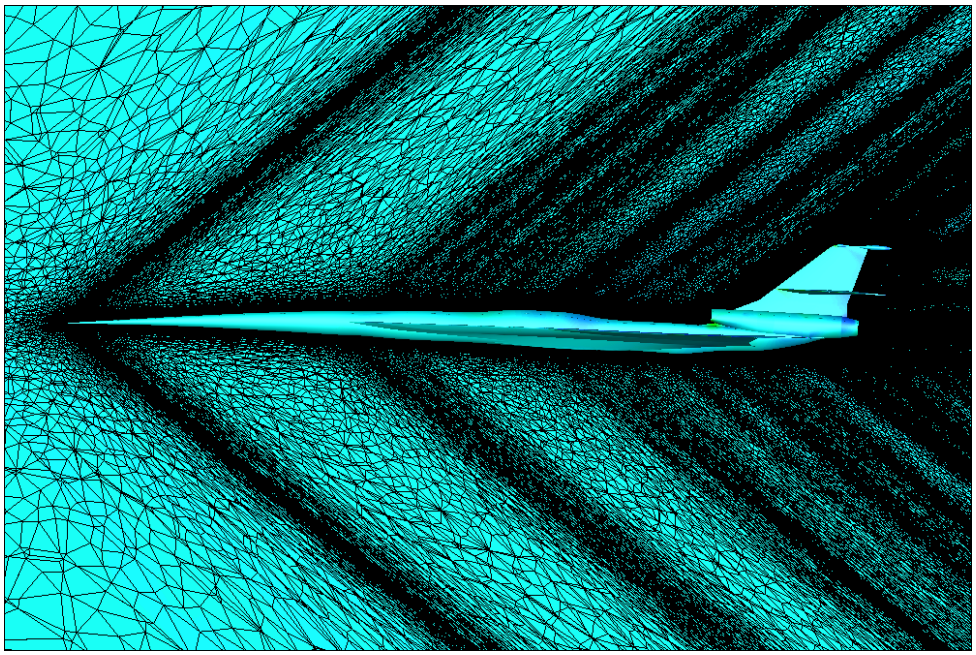

Figure 8: Wake region and sonic boom visualization at y=0

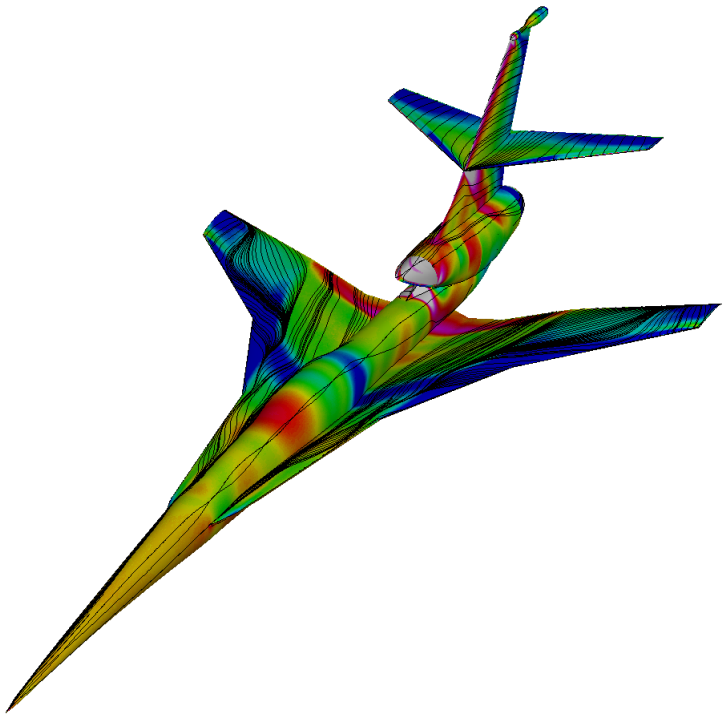

Figure 9: Streamtraces on the main body for adapted mesh

CONCLUSION AND FUTURE WORK

In this paper, numerical results are presented for NASA-C25F model with and without mesh adaptation. Firstly, the numerical model is validated with the benchmark data (Park et al., 2019). Thereafter, the mesh adaptation approach is utilized using an initial mesh in order to improve the accuracy of results. The boundary layer creation and the mesh refinements are performed to capture wake regions, shocks and boundary layers. All refinement process is managed with the pyAMG algorithm using the SU2 solver. More recently the pyAMG algorithm is integrated with the HEMLAB code as well. Yet the adapted results yet to be completed. It has been experienced that numerical convergence are strongly dependent to CFL number, time step size and initial conditions. As can be seen in the results obtained, the current refinement process leads to significant improvements.

ACKNOWLEDGEMENT

The authors also gratefully acknowledge the use of the computing resources provided by the National Center for High Performance Computing of Turkey (UYBHM) under grant number 10752009, and the computing facilities at TUBITAK ULAKBIM, High Performance and Grid Computing Center. The authors also acknowledge the use of the PRACE – Partnership for Advanced Computing in Europe (DECI-16) resources through the Computing Center of the Slovak Academy of Sciences supercomputing infrastructure acquired in project ITMS 26230120002 and 26210120002 (Slovak infrastructure for high-performance computing) supported by the Research & Development Operational Programme funded by the ERDF.

References

Akkurt, S. and Sahin, M. (2017) *An efficicient data structure for three-dimensional vertex based finite volume method,* APS 70th Annual Meeting Division of Fluid Dynamics, November 2017.

Anderson, W. K., Wood, S. L. and Allmaras, S. R. (2019) *An initial exploration of improved numerics within the guidelines of the negative Spalart-Allmaras turbulence model,* NASA/TM, November 2019.

Anderson, G. R., Aftosmis, M. J., and Nemec, M. (2019) *Cart3D Simulations for the Second AIAA Sonic Boom Prediction Workshop,* Journal of Aircraft, Vol 56, p: 896-911, August 2018.

Balay, S., Abhyankar, S., Adams, M. F., et al. (2018) *PETSc Users Manual,* ANL-95/11 - Revision 3.10, Mathematic and Computer Science Division, Argonne National Laboratory, http://www.mcs.anl.gov/petsc, November 2020.

Becker, G. G. and Granzoto, R. M. (2018) *DPW-6 and HiLiftPW-3 using the Stanford university unstructured (SU2),* AIAA Aviation Forum, June 2018.

Karypis, G. and Kumar, V. (1998) *A fast and high quality multilevel scheme for partitioning irregular graphs,* SIAM J. Sci. Comput. Vol 20, p: 359-392, August 1998.

Loseille, A. (2014) *Metric-orthogonal anisotropic mesh generation,* Journal of Aircraft, Vol 56, p: 403-415, October 2014.

Mavriplis, D. J., Vassberg, J. C., Tinoco, E. N., Mani, M., Brodersen, O. P., Eisfeld, B., Wahls, R. A., Morisson, J. H., Zickuhr, T., Levy, D. and Murayama, M. (2008) *Grid quality and resolution issues from the drag prediction workshop series,* 46th AIAA Aerospace Sciences Meeting and Exhibit, 7 - 10 January 2008.

Park, M. A., Balan, A., Anderson, W. K., Galbraith, M. C., Caplan, P. C., Carson, H. A., Michal, T., Krakos, J. A., Kamenetskiy, D. S., Loseille, A., Alauzet, F., Frazza, L. and Barral, N. (2019) *Verification of unstructured grid adaptation components,* AIAA Aerospace Scitech Forum, January 2019.

Park, M. A., and Nemec, M. (2019) *Nearfield summary and statistical analysis of the second AIAA sonic boom prediction workshop,* Journal of Aircraft, Vol 56, p: 851-875

Park, M. A., Kleb, W. L., Jones, W. T., Krakos, J. A., Michal, T. R., Loseille, A., and Dannenhoffer, J. (2019) *Geometry Modeling for Unstructured Mesh Adaptation,* AIAA Aviation Forum, p: 2946, June 2019.

Spalart, P. R. and Allmaras, S. R. (1994) *A one-equation turbulence model for aerodynamic flows,* 30th Aerospace Sciences Meeting & Exhibit, Vol 1, p: 5-21, 6-9 January 1992.

Sukas, H. and Sahin. M, (2021) *HEMLAB algorithm applied to the high-lift JAXA standard model,* AIAA Scitech 2021 Forum, 11–15 & 19–21 January 2021.